



Article

Interface Trap-Induced Temperature Dependent Hysteresis and Mobility in β -Ga₂O₃ Field-Effect Transistors

Youngseo Park ¹, Jiyeon Ma ², Geonwook Yoo ^{2,*} and Junseok Heo ^{1,*}

¹ Department of Electrical and Computer Engineering, Ajou University, Suwon 16499, Korea; pys8685@ajou.ac.kr

² School of Electronic Engineering, Soongsil University, Seoul 06938, Korea; jiyeonma0@gmail.com

* Correspondence: gwyo0@ssu.ac.kr (G.Y.); jsheo@ajou.ac.kr (J.H.); Tel.: +82-31-219-3717 (G.Y.)

Abstract: Interface traps between a gate insulator and beta-gallium oxide (β -Ga₂O₃) channel are extensively studied because of the interface trap charge-induced instability and hysteresis. In this work, their effects on mobility degradation at low temperature and hysteresis at high temperature are investigated by characterizing electrical properties of the device in a temperature range of 20–300 K. As acceptor-like traps at the interface are frozen below 230 K, the hysteresis becomes negligible but simultaneously the channel mobility significantly degrades because the inactive neutral traps allow additional collisions of electrons at the interface. This is confirmed by the fact that a gate bias adversely affects the channel mobility. An activation energy of such traps is estimated as 170 meV. The activated trap charges' trapping and de-trapping processes in response to the gate pulse bias reveal that the time constants for the slow and fast processes decrease due to additionally activated traps as the temperature increases.

Keywords: β -Ga₂O₃; interface trap; hysteresis; mobility degradation; acceptor-like trap



Citation: Park, Y.; Ma, J.; Yoo, G.; Heo, J. Interface Trap-Induced Temperature Dependent Hysteresis and Mobility in β -Ga₂O₃ Field-Effect Transistors. *Nanomaterials* **2021**, *11*, 494. <https://doi.org/10.3390/nano11020494>

Received: 5 January 2021

Accepted: 15 February 2021

Published: 16 February 2021

Publisher's Note: MDPI stays neutral with regard to jurisdictional claims in published maps and institutional affiliations.



Copyright: © 2021 by the authors. Licensee MDPI, Basel, Switzerland. This article is an open access article distributed under the terms and conditions of the Creative Commons Attribution (CC BY) license (<https://creativecommons.org/licenses/by/4.0/>).

1. Introduction

Beta-gallium oxide (β -Ga₂O₃) is a promising material for power semiconductors due to its superior electrical characteristics, such as a direct wide bandgap (4.6–4.9 eV) [1–4], a high electric breakdown field (~8 MV/cm) [5–7], a high electron saturation velocity (~2 × 10⁷ cm/s) [8], high carrier mobility (~100 cm²/V·s) [9–11], and thermal/chemical stability [12–14]. Furthermore, β -Ga₂O₃ exhibits the highest Baliga figure of merit (BFoM; defined as $\epsilon\mu E_G^3$, where ϵ is the dielectric constant, μ is the mobility, and E_G is the bandgap of the semiconductor) [15–17] among wide bandgap semiconductors: the BFoM represents a material parameter related to device power dissipation and the value of β -Ga₂O₃ is approximately ten times and four times higher than those of silicon carbide and gallium nitride, respectively [18,19].

Owing to these attractive characteristics, β -Ga₂O₃ has attracted much interest in a variety of potential applications such as high power transistors [5,7,10], chemical sensors [20], solar-blind ultraviolet (UV) detectors [13,21,22], UV astronomy, and space communication which require practical operation in harsh environments [12]. Thus, in recent times, doping methods [11,23], metal contacts [11,24], and large-area film deposition [9,25,26] of β -Ga₂O₃ have been actively investigated. In particular, the study of the interface characteristics between the gate insulator and the channel is of great significance because the charge trapping at the interface is a more fatal component in β -Ga₂O₃ field-effect transistors (FETs) than bulk traps, and consequently inhibits the high performance and reliability of the devices [27]. Therefore, understanding and controlling the defects at the interface is a critical step in the application of β -Ga₂O₃-based devices. Recent studies have reported on the observation of interface traps in β -Ga₂O₃ metal-oxide-semiconductor (MOS) capacitors and FETs using various gate insulators [8,27,28]. However, previous studies have not revealed

the role of the interface traps in practical devices such as FETs or explicitly described their consequences on device operation.

Herein, we show that the interface trap induces hysteretic behavior in β -Ga₂O₃ FETs at high temperatures and also mobility degradations at low temperatures. To analyze the mobility degradation and hysteresis, a bottom-gate β -Ga₂O₃ FET was fabricated on SiO₂ in this study. The trapping/de-trapping processes at the interface between β -Ga₂O₃ and SiO₂ and their effects on the mobility in the β -Ga₂O₃ FET were studied by analyzing temperature-dependent electrical characteristics in the temperature range of 20–300 K. Additionally, trap-related parameters including the activation trap energy of the interface traps and the trapped charge densities were extracted by means of temperature-dependent hysteresis and transient analysis. This work will expand our understanding of the temperature-dependent characteristics and physical origin of the trap charges in β -Ga₂O₃ FETs.

2. Experiments

2.1. Device Fabrication

The (−201) surface β -Ga₂O₃ bulk substrate with unintentional n-type doping was purchased from Tamura Corporation, Japan. Multi-layer β -Ga₂O₃ flakes were mechanically transferred using a conventional scotch tape method from the β -Ga₂O₃ bulk substrate onto a heavily doped p-type Si substrate with thermally grown 300 nm SiO₂. The source and drain electrodes were defined on top of the Ga₂O₃ flakes by photolithography, 20/100 nm Ti/Au electron-beam evaporation, and a conventional lift-off process. The fabricated device was annealed at 450 °C in nitrogen ambient for 1 min using a rapid thermal process to improve contact resistance.

2.2. Temperature-Dependent Electrical Measurements

The fabricated device was mounted in a liquid helium closed-cycle cryostat (Janis Research, CCS-150, Woburn, MA, USA). Temperature-dependent electrical characteristic measurements were carried out in a high vacuum (<10^{−3} Pa) with a semiconductor parameter analyzer (Keithley, 4200A-SCS, Solon, OH, USA) to identify the intrinsic effects without ambient environmental effects like water and oxygen molecules. To obtain the transfer curves, the gate bias (V_{GS}) was swept from −40 to 10 V (forward sweep) and then back to −40 V (backward sweep) while maintaining drain bias (V_{DS}) values of 0.5 and 1 V. The output characteristics were measured by sweeping V_{DS} from 0 to 10 V while varying the V_{GS} (−15, −10, −5, 0, 5, and 10 V). The transient response was measured by the alternate V_{GS} at a fixed V_{DS} of 1 V. To reach equilibrium, we first applied V_{GS} of 10 V for 600 s until I_{DS} was saturated. Gate pulses were then changed from 10 V to 0 V and maintained for 150 s, and vice versa.

2.3. Contact Resistance, Mobility, and Threshold Voltage Extraction

The contact resistance (R_C) was calculated as follows: $R_C = L \cdot \theta / (W \cdot C_{OX} \cdot \mu_0)$, where θ is the effective mobility attenuation factor, W is the channel width, L is the channel length, C_{OX} is the capacitance of the SiO₂, and μ_0 is the low-field mobility [29]. The low-field mobility was extracted from the Y-function, given by $Y = (\mu_0 \cdot C_{OX} \cdot V_{DS} \cdot W / L)^{0.5} (V_{GS} - V_{th,Y})$, where $V_{th,Y}$ was the threshold voltage extracted from Y-function. The effective mobility attenuation factor was extracted as follows:

$$I_{DS} = \left(\frac{\mu_0}{1 + \theta(V_{GS} - V_{th,Y})} \right) C_{OX} \frac{W}{L} (V_{GS} - V_{th,Y}) V_{DS} \quad (1)$$

We extracted the contact resistance and the mobility from the same transfer curve measured at $V_{DS} = 1$ V. The mobility was extracted from the transfer characteristics. To observe the mobility except for the effect of contact resistance, we first extracted the actually applied drain voltage in the channel ($V_{DS,CH}$) as follows: $V_{DS,CH} = V_{DS} - R_C \times I_{DS}$. Subsequently, the field-effect mobility was calculated as $\mu_{FE} = L \cdot g_m / (W \cdot C_{OX} \cdot V_{DS,CH})$, where g_m is the transconductance. We estimated the threshold voltage as the x -intercept of

the tangential line at the maximum slope on the transfer curve on a linear scale (Figure S1 in Supplementary Materials).

2.4. The Interface Trap Density, the Amount of Charge, Time-Dependent Trapped Charge Density Changes, and Trap Parameter Extraction

The interface trap density is estimated from $SS = \ln(10) \cdot kT/q \cdot (1 + (C_S + C_{it})/C_{OX})$, where SS is the subthreshold swing, C_S is the capacitance of β -Ga₂O₃ conducting channel and $C_{it} = q^2 \times D_{it}$ is the capacitance induced by the interface trap density [4,30]. The amount of charge trapped and de-trapped by the interface trap is extracted as $\Delta Q_{hy} = C_{OX} \times \Delta V$. To determine the activation energy of the interface trap, ΔQ_{hy} was fitted by $\Delta Q_{hy} = Q_m \times \exp(-E_A/k_B T) + Q_{fix}$, where Q_m is the maximum charge density, k_B is the Boltzmann constant, and Q_{fix} is the temperature-independent fixed charge density [30].

The time-dependent density of the trapped charges changes is expressed as $Q_{it}(t) - Q_{it}(0) = -(I_{DS}(t) - I_{DS}(0)) \varepsilon \cdot \varepsilon_0 / q \cdot t_{OX} \cdot g_m$, where $Q_{it}(t)$ is the density of trapped charges (Q_{it}) as a function of time, $Q_{it}(0)$ is Q_{it} at the time changed the gate pulses, $I_{DS}(t)$ is I_{DS} as a function of time, $I_{DS}(0)$ is I_{DS} at the edge of gate pulses, ε is the relative dielectric constant of the oxide, ε_0 is the permittivity of vacuum, and t_{OX} is the thickness of the oxide. The transient $Q_{it}(t) - Q_{it}(0)$ is fitted with a bi-exponential equation: $Q_{it}(t) - Q_{it}(0) = Q_1 \cdot \exp(-t/\tau_{it1}) + Q_2 \cdot \exp(-t/\tau_{it2})$, where Q_1 and Q_2 are the density of trapped charges and τ_{it1} and τ_{it2} are the time constants [26].

3. Results and Discussion

The schematic in Figure 1a shows the fabricated β -Ga₂O₃ FET on a heavily doped p-type Si substrate as the bottom gate with SiO₂ gate insulator. SiO₂ is potentially of a higher dielectric reliability in FETs due to the larger conduction band offset between SiO₂ and Ga₂O₃ compared to Al₂O₃ and Ga₂O₃ [28]. Figure 1b shows an optical microscope image of the fabricated β -Ga₂O₃ device, and we measured W as 3.3 μ m and L as 15 μ m. A thickness of the β -Ga₂O₃ channel layer was measured as approximately 200 nm using atomic force microscopy (the inset in Figure 1b). A cross-sectional high resolution transmission electron microscopy (HR-TEM) image in Figure 1c represents the smooth interface between β -Ga₂O₃ and SiO₂. Mechanical exfoliation of β -Ga₂O₃ and subsequent transfer on SiO₂ did not result in any damage or defect, and a high quality of crystalline was preserved in the fabricated device. The selective-area diffraction pattern was also characterized as shown in Figure 1d. [200] and [002] directions in monoclinic crystal structure were indicated, and the channel surface was confirmed as the β -Ga₂O₃(100) plane.

The fabricated β -Ga₂O₃ FET was characterized by measuring its current-voltage characteristics. Figure 2a,b presents the measured transfer and output characteristics at room temperature, respectively. The fabricated device operates in depletion mode. We extracted the mobility, subthreshold swing, and threshold voltage of the device at room temperature from the transfer characteristics. At $V_{DS} = 1$ V, maximum μ_{FE} of the β -Ga₂O₃ FET were 83.5 and 88.3 cm²/V·s, SS were 180 and 130 mV/dec, and threshold voltages (V_{th}) were -15.5 and -14 V for forward and backward sweeps, respectively, and an ON/OFF ratio (I_{ON}/I_{OFF}) of approximately 10⁷ was observed. Hysteresis (~ 1.5 V), a threshold voltage difference in the transfer curves depending on the sweep directions, was observed. The D_{it} was estimated to be approximately 1.44×10^{11} cm⁻²eV⁻¹ from SS at 300 K. The D_{it} extracted in this work is similar to the previously other reports [27,28]. We also confirmed Ohmic contact behaviors from good linearity of the output curves near 0 V (Figure S2 in Supplementary Materials).

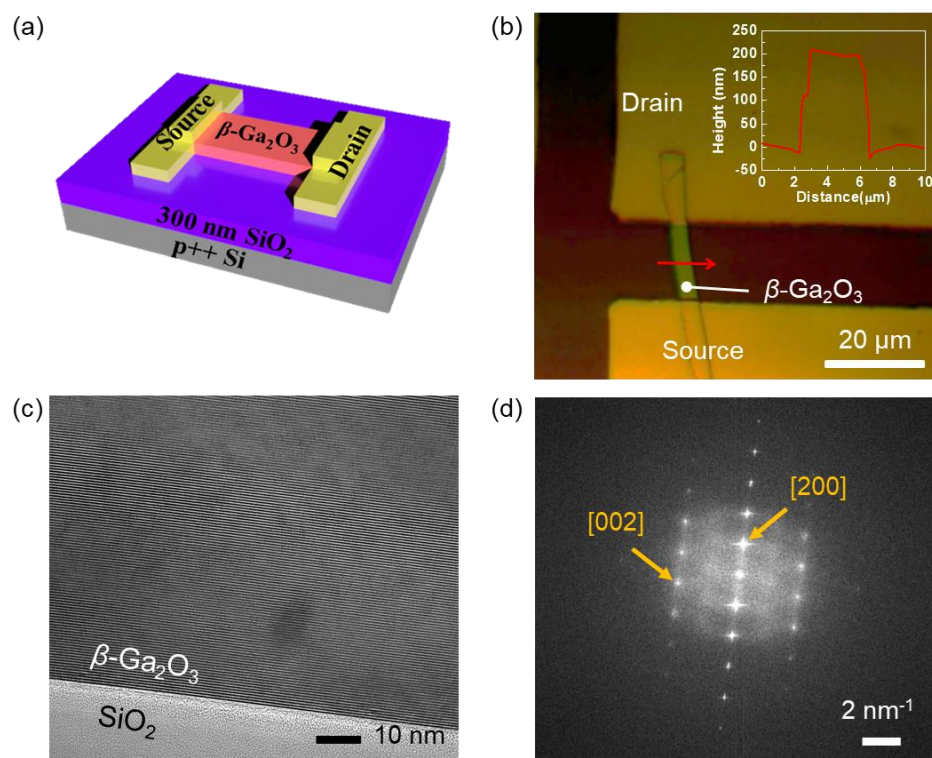


Figure 1. (a) Schematic of the β -Ga₂O₃ field-effect transistor, (b) Optical microscopy image of the fabricated field-effect transistor. The β -Ga₂O₃ channel thickness along the red line was characterized by atomic force microscopy, and the profile is shown in the inset. (c) Cross-sectional HR-TEM image of the interface between β -Ga₂O₃ channel and SiO₂ insulator. (d) Selective area electron diffraction pattern of the β -Ga₂O₃.

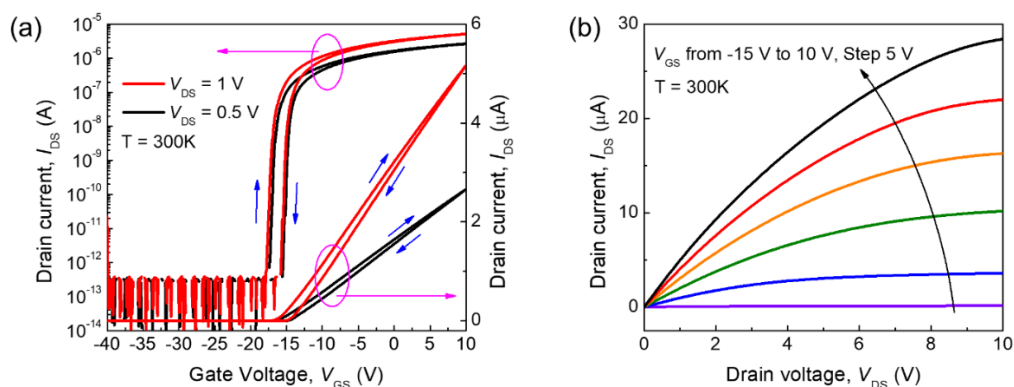


Figure 2. Characteristics of the fabricated β -Ga₂O₃ field-effect transistor: (a) transfer characteristics for $V_{DS} = 0.5$ (black line) and 1 V (red line) at room temperature (V_{GS} was swept from -40 to 10 V (forward sweep) and then back to -40 V (backward sweep)), and (b) output characteristics for $V_{GS} = -15, -10, -5, 0,$ and 5 V at room temperature of the fabricated β -Ga₂O₃ field-effect transistor.

The temperature-dependent hysteretic behaviors of two-dimensional materials were previously reported by our group [30], and in general, it is prevalent that the interface traps and associated charges are responsible for it. Therefore, to investigate the origin of the hysteresis in the β -Ga₂O₃ FET in detail, its temperature dependence was characterized. Figure 3a,b presents the respective transfer curves for forward and backward sweeps at various temperatures from 20 to 300 K, and two properties were observed from the temperature-dependent transfer curves. First, the drain on-current (above the threshold) decreased by

approximately three orders of magnitude as the temperature varied from 20–300 K. Decreasing the temperature would have contributed to the mobility decrease, and a detailed discussion on this follows later on. Second, as the temperature increased, the threshold voltage in the forward sweep shifted more toward a negative value than the one in the backward sweep. In other words, the hysteresis increased as the temperature increased.

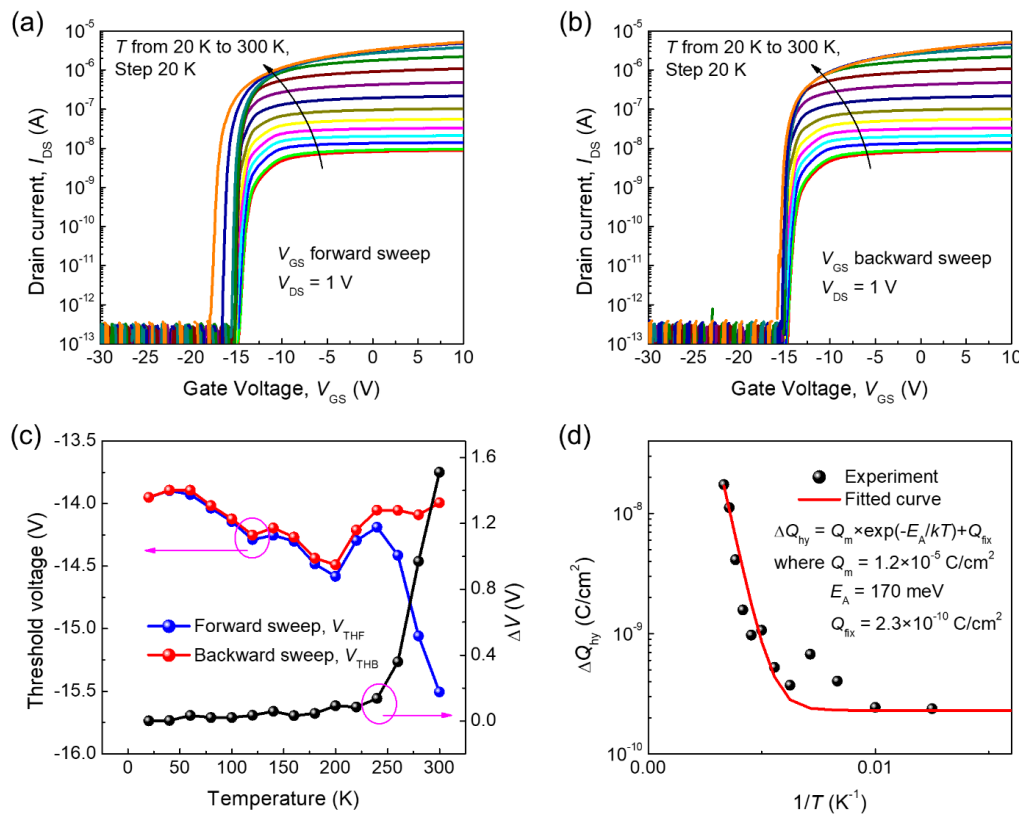


Figure 3. Transfer characteristics of the fabricated β -Ga₂O₃ field-effect transistor: (a) forward sweep and (b) backward sweep at various temperatures from 20 to 300 K, (c) the temperature-dependent threshold voltage in the forward (blue) and backward (red) sweeps and the temperature-dependent degree of hysteresis (black; the difference between the threshold voltages in the forward and backward sweeps), and (d) Arrhenius plots of the ΔQ_{hy} trapped and de-trapped by the interface traps (the red solid line is the best fit of ΔQ_{hy}).

To analyze the hysteresis, we extracted the threshold voltage from the temperature-dependent transfer curves. Figure 3c shows the variations of the V_{th} (left) in the forward (V_{THF} , blue) and backward (V_{THB} , red) sweeps. For consistency, we applied the same method to extract the threshold voltages for different temperatures. Thus, despite the monotonic left-shift of the transfer curves as the temperature increased, the additional change of slope on a linear scale made the variations of the extracted threshold voltage look more or less random and uncorrelated with temperature. Since the degree of hysteresis (ΔV) is defined as the difference between V_{THF} and V_{THB} , any artifact made while obtaining an individual threshold voltage would be canceled out. As shown in Figure 3c, the variations in ΔV below 230 K were almost negligible but started to increase at around 230 K and rose sharply above 230 K due to the thermal activation of the interface traps and the associated charges responsible for the hysteresis. For a more quantitative analysis, the ΔQ_{hy} trapped and de-trapped by the interface trap was extracted and then fitted by an Arrhenius plot, as shown in Figure 3d. The best fit of ΔQ_{hy} was obtained with the fitting parameter values of $Q_m = 1.2 \times 10^{-5}$ C/cm², $E_A = 170$ meV, and $Q_{fix} = 2.3 \times 10^{-10}$ C/cm² (see the Methods section for more detail). The interface trap is partially active at room temperature even if the activation energy of 170 meV is six to seven times greater than the thermal

energy at room temperature. Q_{fix} , the charge density irrespective of the temperature, is five orders of magnitude smaller than Q_{m} . In other words, most of the interface trap charges responsible for the hysteresis are governed by the temperature. In addition to the temperature-dependent hysteresis, the drain current (I_{DS}) decreased in the transfer curve because the mobility is reduced with decreasing temperature, and this temperature-dependent current drop was also observed in the output characteristics. As shown in Figure 4a, the saturation I_{DS} decreased and the slope in the linear region decreased with decreasing temperature, due to an increase in contact resistance (R_{C}) and a decrease in mobility. As can be seen, the I_{DS} no longer showed linear dependence on the bias near the low V_{DS} as the temperature decreased, and the R_{C} values were no longer negligible at low temperature. We extracted the R_{C} from the modified Ghibaudo Y-function method [29] and the mobility by considering the finite R_{C} (see the Methods section for more details). The temperature-dependent R_{C} was calculated for forward and backward sweeps of the transfer curve, as shown in Figure 4b. R_{C} was 6.3 k Ω at 300 K and then rapidly increased up to 100.8 M Ω as the temperature decreased, possibly because of the reduced thermal energies of carriers for thermionic emission over the Schottky barrier.

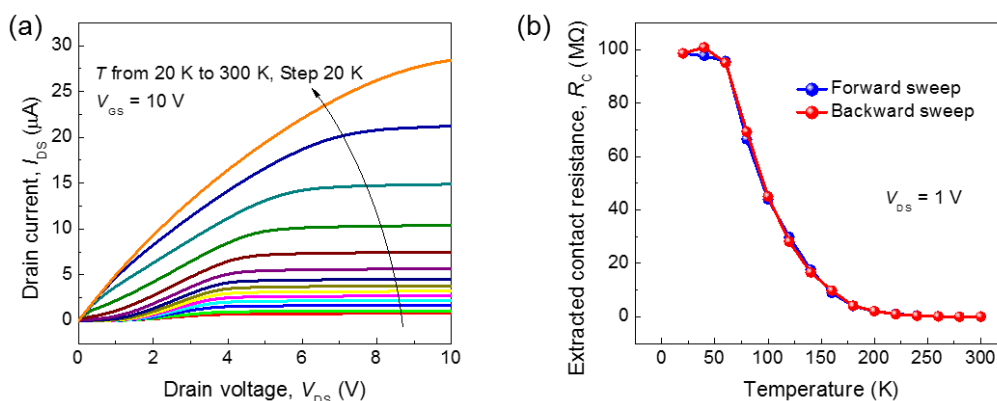


Figure 4. (a) Output characteristics at a gate bias (V_{GS}) of 10 V in the temperature range of 20–300 K and (b) extracted contact resistance at $V_{\text{DS}} = 1 \text{ V}$ of the fabricated $\beta\text{-Ga}_2\text{O}_3$ field-effect transistor in the forward (blue) and backward (red) sweeps.

The maximum channel mobilities (μ_{CH}) at various temperatures considering the effect of the contact resistance are plotted on a log-log scale in Figure 5a. It is worth noting that the channel mobility steeply decreased as the temperature decreased below 230 K. At low temperature (generally below 100 K), the mobility reduced due to the impurity scattering and became proportional to T^γ ($\gamma = 1.5$) as the reported Hall mobility [23,25,31,32] but here it decreased more quickly with γ at approximately 2.2 ($T = \sim 150 \text{ K}$) and 5.6 ($T = 150\text{--}230 \text{ K}$). Thus we cannot explain this mobility degradation by the impurity scattering, and the surface related scattering would be responsible for it. In Figure 5b–e, the transfer curves at $T = 100, 180, 260,$ and 300 K are plotted on a linear scale, respectively, and the extracted channel mobilities in each are also shown alongside. Implausibly, I_{DS} at 100 K rapidly saturated at just above the threshold whereas that at 300 K increased linearly. That is to say, the channel mobility became less affected by the gate bias as the temperature increased. Interestingly, the channel mobility started to decrease below 230 K (the temperature that coincides with the hysteresis becoming invisible). Therefore, these trends contributed to the interplay between interface scattering and the effect of acceptor-like traps at the interface between $\beta\text{-Ga}_2\text{O}_3$ and SiO_2 [27]. At temperatures below 230 K, the acceptor-like traps were frozen and electrically neutral, allowing more electrons to drift along the vicinity of the interface. The interface scattering became predominant over any other scatterings including ionized impurity scattering, and mobility steeply decreased. This can also be envisioned by the strong gate bias dependence of the channel mobility at low temperature,

as discussed earlier (Figure 5b), and the previous reports of strong mobility degradation by the surface effects in β -Ga₂O₃ thin-films at low temperatures [33].

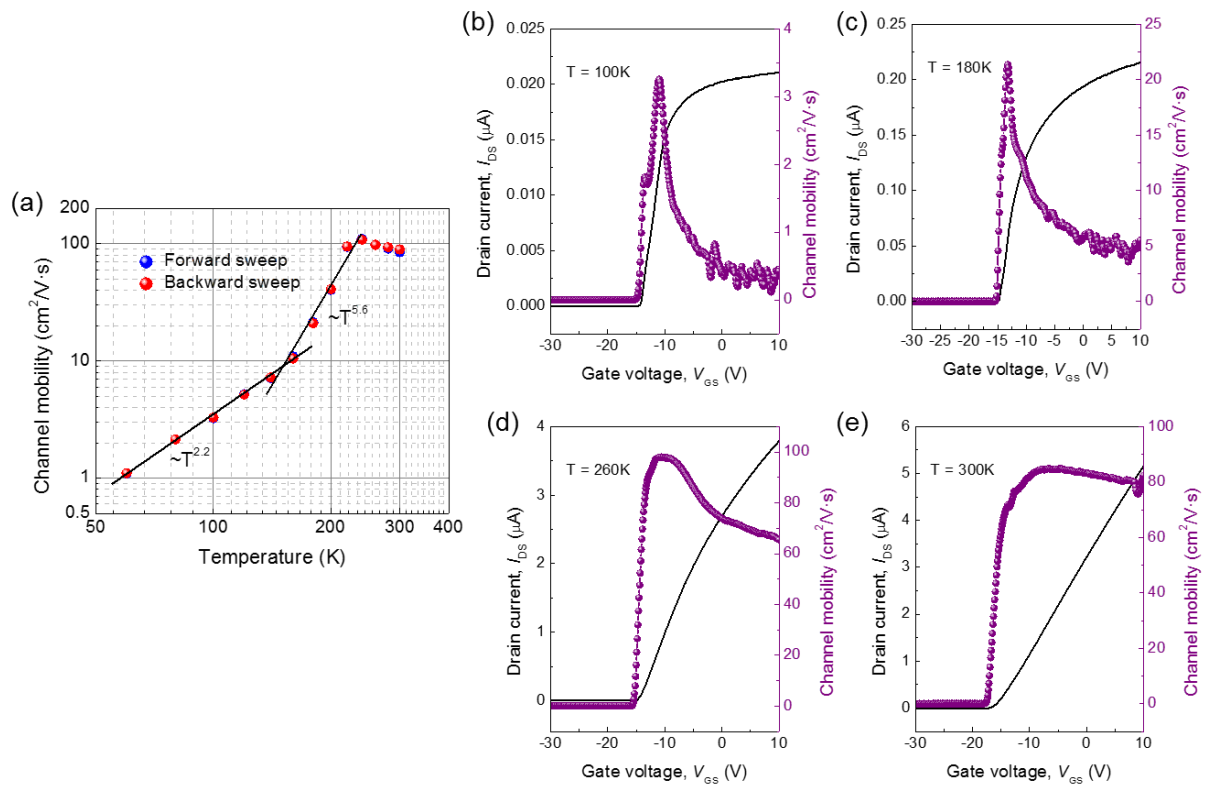


Figure 5. (a) Maximum channel mobilities at various temperatures ($T = 60$ – 300 K) on a log-log scale (the black solid lines are the fitted channel mobilities proportional to approximately $T^{2.2}$ ($T = \sim 150$ K) and $T^{5.6}$ ($T = 150$ – 230 K)) and (b–e) transfer curves on a linear scale for $T = 100$, 180, 260, and 300 K with the extracted channel mobilities of the fabricated β -Ga₂O₃ field-effect transistor.

We also carried out a time-domain analysis on the capture and release of charges by the traps at the interface by measuring the transient response to observe the behaviors of the traps [34]. As shown in Figure 6a, as soon as V_{GS} dropped, I_{DS} sharply dropped and then slowly increased because the captured carriers were released from the interface traps. At the rising edge of V_{GS} , I_{DS} popped up and then slowly decreased while maintaining V_{GS} because of the electrons captured by the acceptor-like traps at the interface. As the temperature increased, these phenomena noticeably appeared because more of the acceptor-like traps were activated. We calculated the transient changes of the trapped charge density for the temperature from 240 to 320 K, as shown in Figure 6b; as the temperature increased, the changes of trapped and de-trapped charge density also increased. The transient changes were not observed below 240 K because of negligible variation by the trapped charge. Figure 6c shows temperature-dependent time constants extracted by fitting Figure 6b with a bi-exponential equation [35]. All of the time constants for the slow and fast processes decreased as the temperature increased because the activated traps were more abundant and the electrons were more thermally energized. We also observed that the charge trapping processes were faster than the charge de-trapping processes. The detailed time constants are available in the Supplementary Materials (Table S1).

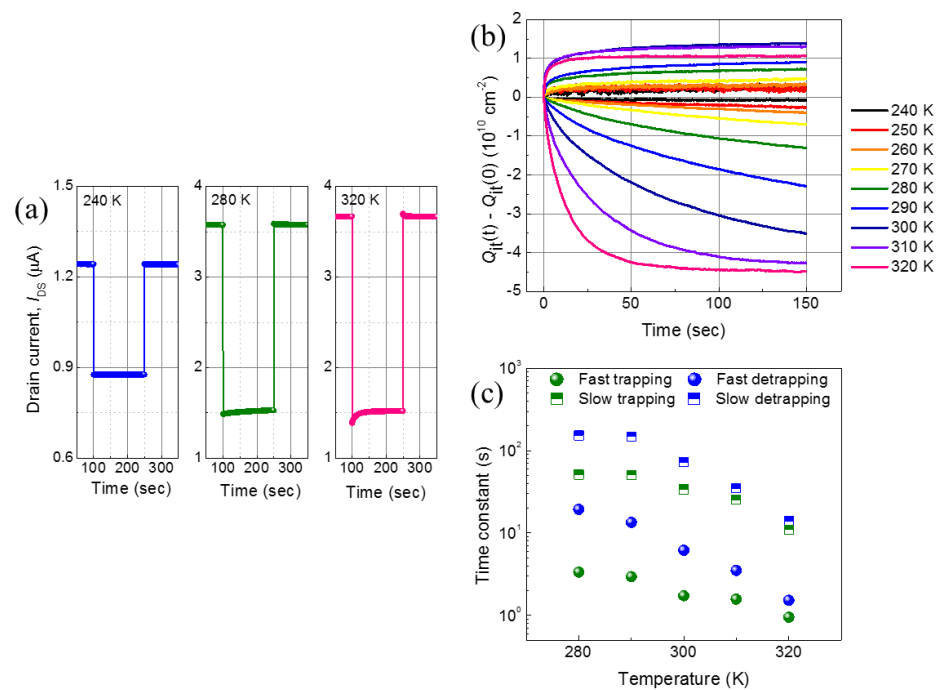


Figure 6. (a) Transient responses of I_{DS} to the V_{GS} changes at $T = 240, 280,$ and 320 K, (b) changes of trapped charge density as a function of time from 240 to 320 K, and (c) the extracted temperature-dependent time constants for the slow and fast processes of the fabricated $\beta\text{-Ga}_2\text{O}_3$ field-effect transistor.

4. Conclusions

In summary, we investigated the effect of interface traps on the degradation of channel mobility and hysteresis in a bottom-gated $\beta\text{-Ga}_2\text{O}_3$ FET at low temperature. Temperature-dependent electrical characterizations were performed on the device in the temperature range of 20–300 K, and variations in threshold voltage and field-effect mobility and the degree of hysteresis were analyzed. The activation energy of the interface trap between $\beta\text{-Ga}_2\text{O}_3$ and SiO_2 was estimated as 170 meV, and there was no observable hysteresis below 230 K. As the acceptor-like traps at the interface are frozen and inactive at low temperature, the hysteresis disappears and it was simultaneously found that the channel mobility sharply decreases. This was understood as the frozen charged traps allow the channel electrons to collide at the interface, which was also confirmed by the vulnerability of mobility to gate bias at low temperature. Furthermore, the charge trapping and detrapping processes at the interface were studied in the time-domain by switching the gate bias. At higher temperatures, the extracted time constants for the slow and fast processes became shorter due to more activated traps. We believe that understanding the role of the interface traps between the gate insulator and $\beta\text{-Ga}_2\text{O}_3$ could help to optimize the fabrication and operation of $\beta\text{-Ga}_2\text{O}_3$ -based devices in a variety of circumstances, particularly in harsh environments in space and military applications.

Supplementary Materials: The following are available online at <https://www.mdpi.com/2079-4991/11/2/494/s1>, Figure S1. Transfer curve for $V_{DS} = 1$ V in a linear scale at 180 K, Figure S2. Output curves of I_{DS} -low V_{DS} at room temperature, Table S1. The density of the trapped and de-trapped charges and the time constants.

Author Contributions: Conceptualization: G.Y. and J.H.; methodology: Y.P. and J.M.; formal analysis: Y.P.; investigation: Y.P.; writing—original draft preparation: Y.P. and J.M.; writing—review and editing: G.Y. and J.H.; visualization: Y.P. and J.M.; supervision: G.Y. and J.H.; project administration: J.H.; funding acquisition: J.H. All authors have read and agreed to the published version of the manuscript.

Funding: This study was supported by the Industrial Strategic Technology Development Program (20000300) funded by the Ministry of Trade, Industry, and Energy (MOTIE, Republic of Korea), and Human Resources Program in Energy Technology of the Korea Institute of Energy Technology Evaluation and Planning, granted financial resource from the MOTIE, Republic of Korea (no. 20184030202220).

Data Availability Statement: The data presented in this study are available on request from the corresponding author.

Conflicts of Interest: The authors declare no conflict of interest. The funders had no role in the design of the study; in the collection, analyses, or interpretation of data; in the writing of the manuscript; or in the decision to publish the results.

References

1. Kim, M.; Seo, J.-H.; Singiseti, U.; Ma, Z. Recent advances in free-standing single crystalline wide band-gap semiconductors and their applications: GaN, SiC, ZnO, β -Ga₂O₃, and diamond. *J. Mater. Chem. C* **2017**, *5*, 8338–8354. [[CrossRef](#)]
2. Bhuiyan, M.A.; Zhou, H.; Jiang, R.; Zhang, E.X.; Fleetwood, D.M.; Ye, P.D.; Ma, T. Charge Trapping in Al₂O₃/ β -Ga₂O₃-Based MOS Capacitors. *IEEE Electron Device Lett.* **2018**, *39*, 1022–1025. [[CrossRef](#)]
3. Nagarajan, L.; De Souza, R.A.; Samuelis, D.; Valov, I.; Börger, A.; Janek, J.; Becker, K.-D.; Schmidt, P.C.; Martin, M. A chemically driven insulator–metal transition in non-stoichiometric and amorphous gallium oxide. *Nat. Mater.* **2008**, *7*, 391–398. [[CrossRef](#)]
4. Zhou, H.; Maize, K.; Noh, J.; Shakouri, A.; Ye, P.D. Thermodynamic Studies of β -Ga₂O₃ Nanomembrane Field-Effect Transistors on a Sapphire Substrate. *ACS Omega* **2017**, *2*, 7723–7729. [[CrossRef](#)] [[PubMed](#)]
5. Ma, J.; Lee, O.; Yoo, G. Effect of Al₂O₃ Passivation on Electrical Properties of β -Ga₂O₃ Field-Effect Transistor. *IEEE J. Electron Devices Soc.* **2019**, *7*, 512–516. [[CrossRef](#)]
6. Pozina, G.; Forsberg, M.; Kaliteevski, M.A.; Hemmingsson, C. Emission properties of Ga₂O₃ nano-flakes: Effect of excitation density. *Sci. Rep.* **2017**, *7*, 42132. [[CrossRef](#)]
7. Ma, J.; Lee, O.; Yoo, G. Abnormal Bias-Temperature Stress and Thermal Instability of β -Ga₂O₃ Nanomembrane Field-Effect Transistor. *IEEE J. Electron Devices Soc.* **2018**, *6*, 1124–1128. [[CrossRef](#)]
8. Polyakov, A.Y.; Smirnov, N.B.; Shchemerov, I.V.; Chernykh, S.V.; Oh, S.; Pearton, S.J.; Ren, F.; Kochkova, A.; Kim, J. Defect States Determining Dynamic Trapping-De trapping in β -Ga₂O₃ Field-Effect Transistors. *ECS J. Solid State Sci. Technol.* **2019**, *8*, Q3013–Q3018. [[CrossRef](#)]
9. Higashiwaki, M.; Sasaki, K.; Murakami, H.; Kumagai, Y.; Koukita, A.; Kuramata, A.; Masui, T.; Yamakoshi, S. Recent progress in Ga₂O₃ power devices. *Semicond. Sci. Technol.* **2016**, *31*, 34001. [[CrossRef](#)]
10. Higashiwaki, M.; Sasaki, K.; Kuramata, A.; Masui, T.; Yamakoshi, S. Gallium oxide (Ga₂O₃) metal-semiconductor field-effect transistors on single-crystal β -Ga₂O₃ (010) substrates. *Appl. Phys. Lett.* **2012**, *100*, 13504. [[CrossRef](#)]
11. Sasaki, K.; Higashiwaki, M.; Kuramata, A.; Masui, T.; Yamakoshi, S. Si-Ion Implantation Doping in β -Ga₂O₃ and Its Application to Fabrication of Low-Resistance Ohmic Contacts. *Appl. Phys. Express* **2013**, *6*, 86502. [[CrossRef](#)]
12. Tak, B.R.; Garg, M.; Kumar, A.; Gupta, V.; Singh, R. Gamma Irradiation Effect on Performance of β -Ga₂O₃ Metal-Semiconductor-Metal Solar-Blind Photodetectors for Space Applications. *ECS J. Solid State Sci. Technol.* **2019**, *8*, Q3149–Q3153. [[CrossRef](#)]
13. Oh, S.; Kim, J.; Ren, F.; Pearton, S.J.; Kim, J. Quasi-two-dimensional β -gallium oxide solar-blind photodetectors with ultrahigh responsivity. *J. Mater. Chem. C* **2016**, *4*, 9245–9250. [[CrossRef](#)]
14. Guo, D.; An, Y.; Cui, W.; Zhi, Y.; Zhao, X.; Lei, M.; Li, L.; Li, P.; Wu, Z.; Tang, W. Epitaxial growth and magnetic properties of ultraviolet transparent Ga₂O₃/(Ga_{1-x}Fe_x)₂O₃ multilayer thin films. *Sci. Rep.* **2016**, *6*, 25166. [[CrossRef](#)] [[PubMed](#)]
15. Zhou, H.; Alghmadi, S.; Si, M.; Qiu, G.; Ye, P.D. Al₂O₃/ β -Ga₂O₃(-201) Interface Improvement Through Piranha Pretreatment and Postdeposition Annealing. *IEEE Electron Device Lett.* **2016**, *37*, 1411–1414. [[CrossRef](#)]
16. Baliga, B.J. Power semiconductor device figure of merit for high-frequency applications. *IEEE Electron Device Lett.* **1989**, *10*, 455–457. [[CrossRef](#)]
17. Wang, H.; Wang, F.; Zhang, J. Power Semiconductor Device Figure of Merit for High-Power-Density Converter Design Applications. *IEEE Trans. Electron Devices* **2008**, *55*, 466–470. [[CrossRef](#)]
18. Swinnich, E.; Hasan, M.N.; Zeng, K.; Dove, Y.; Singiseti, U.; Mazumder, B.; Seo, J.-H. Flexible β -Ga₂O₃ Nanomembrane Schottky Barrier Diodes. *Adv. Electron. Mater.* **2019**, *5*, 1800714. [[CrossRef](#)]
19. Kim, J.; Mastro, M.A.; Tadjer, M.J.; Kim, J. Quasi-Two-Dimensional h-BN/ β -Ga₂O₃ Heterostructure Metal–Insulator–Semiconductor Field-Effect Transistor. *ACS Appl. Mater. Interfaces* **2017**, *9*, 21322–21327. [[CrossRef](#)]
20. Hoefer, U.; Frank, J.; Fleischer, M. High temperature Ga₂O₃-gas sensors and SnO₂-gas sensors: A comparison. *Sens. Actuators B Chem.* **2001**, *78*, 6–11. [[CrossRef](#)]
21. Huang, J.R.; Hsu, W.C.; Chen, Y.J.; Wang, T.B.; Lin, K.W.; Chen, H.I.; Liu, W.C. Comparison of hydrogen sensing characteristics for Pd/GaN and Pd/Al_{0.3}Ga_{0.7}As Schottky diodes. *Sens. Actuators B Chem.* **2006**, *117*, 151–158. [[CrossRef](#)]
22. You, A.; Be, M.A.Y.; In, I. High-performance metal-semiconductor-metal deep-ultraviolet photodetectors based on homoepitaxial diamond thin film. *Appl. Phys. Lett.* **2006**, *89*, 113509.

23. Moser, N.; McCandless, J.; Crespo, A.; Leedy, K.; Green, A.; Neal, A.; Mou, S.; Ahmadi, E.; Speck, J.; Chabak, K.; et al. Ge-Doped β -Ga₂O₃ MOSFETs. *IEEE Electron Device Lett.* **2017**, *38*, 775–778. [[CrossRef](#)]
24. Züttel, A. Materials for hydrogen storage. *Mater. Today* **2003**, *6*, 24–33. [[CrossRef](#)]
25. Zhang, Y.; Alema, F.; Mauze, A.; Koksaldi, O.S.; Miller, R.; Osinsky, A.; Speck, J.S. MOCVD grown epitaxial β -Ga₂O₃ thin film with an electron mobility of 176 cm²/V s at room temperature. *APL Mater.* **2018**, *7*, 22506. [[CrossRef](#)]
26. Sbrokek, N.M.; Salagaj, T.; Coleman, E.; Tompa, G.S.; Moon, Y.; Kim, M.S. Large-Area MOCVD Growth of Ga₂O₃ in a Rotating Disc Reactor. *J. Electron. Mater.* **2015**, *44*, 1357–1360. [[CrossRef](#)]
27. Bae, H.; Noh, J.; Alghamdi, S.; Si, M.; Ye, P.D. Ultraviolet Light-Based Current–Voltage Method for Simultaneous Extraction of Donor- and Acceptor-Like Interface Traps in β -Ga₂O₃ FETs. *IEEE Electron Device Lett.* **2018**, *39*, 1708–1711. [[CrossRef](#)]
28. Jayawardena, A.; Ramamurthy, R.P.; Ahyi, A.C.; Morissette, D.; Dhar, S. Interface trapping in (2⁻01) β -Ga₂O₃ MOS capacitors with deposited dielectrics. *Appl. Phys. Lett.* **2018**, *112*, 192108. [[CrossRef](#)]
29. Chang, H.-Y.; Zhu, W.; Akinwande, D. On the mobility and contact resistance evaluation for transistors based on MoS₂ or two-dimensional semiconducting atomic crystals. *Appl. Phys. Lett.* **2014**, *104*, 113504. [[CrossRef](#)]
30. Park, Y.; Baac, H.W.; Heo, J.; Yoo, G. Thermally activated trap charges responsible for hysteresis in multilayer MoS₂ field-effect transistors. *Appl. Phys. Lett.* **2016**, *108*, 83102. [[CrossRef](#)]
31. Kabilova, Z.; Kurdak, C.; Peterson, R.L. Observation of impurity band conduction and variable range hopping in heavily doped (010) β -Ga₂O₃. *Semicond. Sci. Technol.* **2019**, *34*, 03LT02. [[CrossRef](#)]
32. Irmscher, K.; Galazka, Z.; Pietsch, M.; Uecker, R.; Fornari, R. Electrical properties of β -Ga₂O₃ single crystals grown by the Czochralski method. *J. Appl. Phys.* **2011**, *110*, 63720. [[CrossRef](#)]
33. Ahrling, R.; Boy, J.; Handwerg, M.; Chiatti, O.; Mitdank, R.; Wagner, G.; Galazka, Z.; Fischer, S.F. Transport Properties and Finite Size Effects in β -Ga₂O₃ Thin Films. *Sci. Rep.* **2019**, *9*, 13149. [[CrossRef](#)] [[PubMed](#)]
34. Zhang, W.; Zhang, Y.; Mao, W.; Ma, X.; Zhang, J.; Hao, Y. Influence of the Interface Acceptor-Like Traps on the Transient Response of AlGa_N/Ga_N HEMTs. *IEEE Electron Device Lett.* **2013**, *34*, 45–47. [[CrossRef](#)]
35. Guo, Y.; Wei, X.; Shu, J.; Liu, B.; Yin, J.; Guan, C.; Han, Y.; Gao, S.; Chen, Q. Charge trapping at the MoS₂-SiO₂ interface and its effects on the characteristics of MoS₂ metal-oxide-semiconductor field effect transistors. *Appl. Phys. Lett.* **2015**, *106*, 103109. [[CrossRef](#)]